ORIGINAL PAPER

The Brittle–Ductile Transition and the Formation of Compaction Bands in the Savonnières Limestone: Impact of the Stress and Pore Fluid

Mustafa Sari[1] · **Joel Sarout**[2] · **Thomas Poulet**[1] · **Jeremie Dautriat**[2] · **Manolis Veveakis**[3]

Abstract

Carbonate sediments play a prominent role on the global geological stage as they store more than 60% of world's oil and 40% of world's gas reserves. Prediction of the deformation and failure of porous carbonates is, therefore, essential to minimise reservoir compaction, fault reactivation, or wellbore instability. This relies on our understanding of the mechanisms underlying the observed inelastic response to fluid injection or deviatoric stress perturbations. Understanding the impact of deformation/ failure on the hydraulic properties of the rock is also essential as injection/production rates will be affected. In this work, we present new experimental results from triaxial deformation experiments carried out to elucidate the behaviour of a porous limestone reservoir analogue (Savonnières limestone). Drained triaxial and isotropic compression tests were conducted at five different confining pressures in dry and water-saturated conditions. Stress–strain data and X-ray tomography images of the rock indicate two distinct types of deformation and failure regimes: at low confinement (10 MPa) brittle failure in the form of dilatant shear banding was dominant; whereas at higher confinement compaction bands orthogonal to the maximum principal stress formed. In addition to the pore pressure effect, the presence of water in the pore space significantly weakened the rock, thereby shrinking the yield envelope compared to the dry conditions, and shifted the brittle–ductile transition to lower effective confining pressures (from 35 MPa to 29 MPa). Finally, permeability measurements during deformation show a reduction of an order of magnitude in the ductile regime due to the formation of the compaction bands. These results highlight the importance of considering the role of the saturating fluid in the brittle–ductile response of porous rocks and elucidate some of the microstructural processes taking place during this transition.

Highlights

- Triaxial testing and petrophysical characterisation of the Savonnières limestone, an oolithic carbonate reservoir analogue

- Saturation of the pore space with water instead of air reduces the mechanical strength and shrinks the yield envelope
- Compaction bands are observed in the brittle-ductile transition zone using X-ray Computed Tomography
- Compaction bands reduce the permeability of the rock

✉ Mustafa Sari
mustafa.sari@csiro.au

Joel Sarout
joel.sarout@csiro.au

Thomas Poulet
thomas.poulet@csiro.au

Jeremie Dautriat
jeremie.dautriat@csiro.au

Manolis Veveakis
manolis.veveakis@duke.edu

1 Mineral Resources, CSIRO, Kensington 6151, WA, Australia

2 Energy, CSIRO, Kensington 6151, WA, Australia

3 School of Civil and Environmental Engineering, Duke University, Durham 27708, NC, USA

🍀 Springer

1 Introduction

Carbonate sediments play a prominent role on the global geological stage as they store more than 60% of world's oil and 40% of world's gas reserves Schlumberger (2007). The production of oil and gas from carbonate rocks represents 60% of the total production worldwide Roehl and Choquette (1986); Halbouty (2003). They also host more than 50% of the world's deep saline aquifers Gouze and Luquot (2011), often considered safe candidates for effective CO_2 geo-sequestration. Porous carbonate rocks in nature are often mechanically weak, heterogeneous at multiple scales (e.g., vuggy, fractured), sensitive to effective stress changes, and to the chemistry of the fluid saturating the pore space (e.g., water-induced mechanical weakening) (Grgić 2011; Vik et al. 2013; Shulakova et al. 2017; Pimienta et al. 2017). Carbonate reservoirs are, therefore, strongly impacted by typical anthropogenic subsurface operations such as fluid injection (e.g., CO_2 geo-sequestration), or fluid withdrawal (e.g., hydrocarbon production) that perturb the natural state of stress at depth, and alter the chemical equilibrium between the rock frame and the pore fluid.

Changes in the macroscopic properties of the rock are often directly related to changes in its microstructure (e.g., micro-cracking) in response to changes in stress, temperature or pore fluid chemistry, and can lead to macroscopic strain localisation and the formation of fractures, shear bands, or compaction bands (Sari et al. 2020; Stefanou and Sulem 2014). The magnitude and extent of these changes are typically governed by the stress field (magnitude, anisotropy, orientation), the nature of the native pore fluid and that of the injected fluid (rock-fluid interactions), the nature of the rock formation (e.g., mineralogy, microstructure, heterogeneity), and its propensity for strain localisation Sulem and Vardoulakis (1995).

At low effective confining pressure porous carbonates mechanically fail in a brittle manner, which is typically characterised by the development of localised damage and dilatancy under increasing deviatoric compressive stress Paterson and Wong (2005). By increasing the effective pressure, porous carbonates progressively transition toward a ductile deformation regime (e.g.,Baud et al. 2000; Wong and Baud 2012; Kodaka et al. 2017; Leuthold et al. 2021) with more diffuse deformation often associated with strain hardening Baud et al. 2000; Vajdova et al. 2004. The transitional brittle/ductile regime features a mixture of the attributes of the above two end members: diffuse irreversible deformation followed by strain localisation, where yield and strain hardening/softening take place. Compaction bands are a specific yield/failure mode in porous rocks, reportedly occurring in the transitional brittle/ductile deformation regime. In this regime, discrete thin bands orthogonal to the increasing maximum compressive stress can form. Within these bands, a significant porosity/permeability reduction (Dautriat et al. 2009; Dimanov et al. 2011), this reduction is often associated with grain cracking, crushing and reduction in size, concomitant with cataclastic pore collapse and pore size reduction (Papamichos et al. 1993; Sulem and Vardoulakis 1995; Fortin et al. 2005, 2007; Wong et al. 1997; Zhu et al. 2002; Zhang and Spiers 2005; Ghabezloo et al. 2009; Abdallah et al. 2021). Intra-crystalline plasticity of calcite grains (twinning) has also been shown to contribute significantly to the overall volume reduction observed in compaction bands (Baud et al. 2000; Zhu et al. 2010; Issen 2002).

Assuming that the native pore fluid in situ is in equilibrium with the rock-forming minerals, hydro-chemical interactions associated with the injection of a different fluid (e.g., CO_2) can lead to changes in the mechanical (e.g., strength reduction) and hydraulic (e.g., permeability reduction) properties of the rock as well as the elastic/seismic properties of porous rocks (Baud et al. 2000; David et al. 2015), and further affect the overall project economics (Colback and Wiid 1965; Hawkins and McConnell 1992; Vàsàrhelyi 2005; Erguler and Ulusay 2009). Multiple water weakening mechanisms have been reported in the literature, operating at various time scales in different rock types, e.g., adsorption effects at grain surfaces (Orowan 1944; Rebinder et al. 1948; Baud et al. 2000; Pimienta et al. 2017), capillary effects, water- clay mineral interactions (Schmitt et al. 1994; David et al. 2015), mineral solubility (especially in calcite-rich rocks, Risnes et al. (2005)), and stress corrosion at the tip of the fractures/cracks (Atkinson and Meredith 1987; Zhu and Wong 1997). Mechanical weakening can occur with exposure to non-native pore fluids (e.g., fluid injection), the Ekofisk field, Norwegian North sea, is an example of a compacting chalk reservoir with considerable subsequent sea floor subsidence due water weakening (Teufel et al. 1991; Sylte et al. 1999). Fluid-driven mineral dissolution can occur locally in calcite-rich rocks, which will affect the mechanical failure mode at a given mean effective stress (depth) (Zhang and Spiers 2005; Zhang et al. 2010; Croize et al. 2013). Stress corrosion is another mechanism thought to promote the growth of pre-existing cracks in calcite grains, and indirectly affect the characteristics of the brittle–ductile transition Gratier et al. (1999). This suggests that water weakening can affect not only the mechanical strength and elastic/seismic response of the rock, but also the mechanical failure mode, and, therefore, strain localisation and its consequences on reservoir properties.

Evaluating in the laboratory to what extent a fluid affects the mechanical strength, elastic/seismic properties and the mechanical failure mode (strain localisation) of a homogeneous carbonate reservoir analogue is the objective of this work. The impact of compaction bands and other strain localisation phenomena on the permeability of the rock is also evaluated. To this end, a series of conventional (axisymmetric) triaxial tests on multiple and virtually identical cylindrical samples of Savonnières limestone have been conducted in dry and water-saturated (drained) conditions. For comparison purposes, each sample was tested at a different mean effective stress value, covering the brittle and ductile deformation regimes for this particular rock. For all tests, the deviatoric stress loading was applied at the same constant axial displacement rate, sufficiently low to achieve drained conditions everywhere within the water-saturated samples.

2 Materials and Methods

2.1 The Savonnières Limestone

The Savonnières is a Jurassic limestone quarried in the Eastern part of France near the town of Savonnières-en-Perthois (Moh 2008; Fronteau et al. 2010). This shelly oolitic limestone is composed of ellipsoidal ooids and sea shells embedded in a matrix of sparry calcite cement (sparite). The ooids are more or less hollowed out (calcite dissolution) to form oomoldic pores with a characteristic size > 100 μm Qajar et al. (2013). This limestone is made of virtually 100% calcite, and appears made of small, closely woven, grey-beige grains with many vesicles Shulakova et al. (2017) (see Fig. 1a). In terms of microstructure, this limestone is similar to the Brauvilliers limestone, also reported in the literature (e.g., Vo-Thanh 1995; Cadoret et al. 1995; Tserkovnyak and Johnson 2002).

The block of Savonnières limestone available for this study was first imaged with a medical X-ray CT scanner at a resolution of 100 μm x 100 μm x 400 μm per voxel. The

reconstructed 3D density map shows the relative homogeneity of the rock at the cm to dm scale with the available resolution (see Fig. 1b). All rock material used in this work was extracted from this block, including the triaxial test plugs, i.e., cylinders with D = 38mm and L ≈ 76mm. As a consequence, all the samples used for characterisation and testing at the laboratory scale are assumed to be identical and representative of the Savonnières limestone formation. The test plugs were first cored with water acting as the cooling/lubricating fluid, then dried in an oven at 60°C for 48 h. The porosity and permeability at 2 MPa effective pressure of one representative plug extracted from the parent block of Savonnières limestone was evaluated using Nitrogen gas and the pulse-decay technique (CoreTest AP-608 apparatus). The dry density was estimated from the ratio of the dry mass to the bulk volume of the dry rock sample. Note that five repeated measurements were conducted under these conditions to evaluate the associated uncertainty, i.e.,

Porosity: $\quad \phi = 30.48\% \pm 1.44$,

Gas permeability: $\quad k_{gas} = 58.9 \text{ mD} \pm 7.3$,

Bulk density (dry): $\quad \rho_{dry} = 1.887 \text{ g/cm}^3 \pm 0.0015$.

2.2 Laboratory Methods

2.2.1 Characterisation and Testing Procedures

Prior to testing, each rock sample is imaged with a medical X-ray CT scanner at a resolution of 100 μm x 100 μm x 400 μm per voxel. It is then set up within a rubber sleeve and between two steel end-platens in contact with the top and bottom end faces of the sample to avoid contact with the confining oil within the pressure chamber of the triaxial vessel. This arrangement also allows for the independent control of the pore pressure and vertical stress. The pressure chamber is then closed and filled with confining oil. For the

Fig. 1 **a** Scanning Electron Microscope (SEM) images of a representative thin section extracted from the Savonnières limestone block in it natural state Shulakova et al. (2017). **b** CT-scan image of the Savonnières block from which the samples were cored. Note that the geometry of the block generates artefacts on the X-ray particle propagation from each corner of the block, which leads to these visualisation artefacts

(a)

(b)
black areas correspond to the cored samples
40 cm
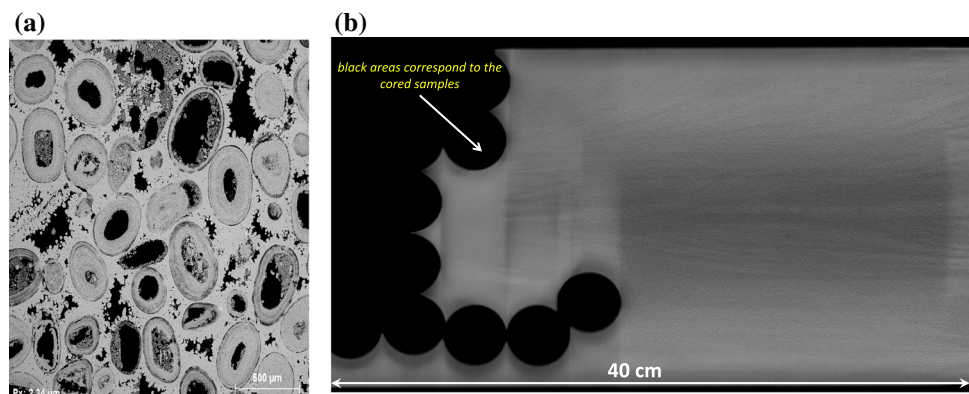
dry samples, confining pressure is increased to achieve the target value for each triaxial test (1, 5, 10, 15, or 22 MPa). The wet samples are water-saturated prior to testing in a desiccator under vacuum for 48 h. After setting them up in the pressure chamber, a low confining pressure of about 0.7 MPa is first applied, then water is flushed through the sample between the bottom and top ends of the sample with a small pressure gradient of 0.4 MPa (low flow rate). This procedure ensures that air potentially trapped within the pore space of the sample and the pore fluid lines is flushed out by displacing several pore volumes of water. The confining and pore pressures are then increased simultaneously but at different rates to achieve the target effective pressure for each test, i.e., the confining pressure target is either 1.5, 5.5, 10.5, 15.5, or 22.5 MPa, while the pore pressure target is always 0.5 MPa.

Once equilibrated at the target effective pressure, an increasing compressive vertical stress is applied along the samples' axis at a constant vertical displacement rate corresponding to a strain rate of about $10^{-5}s^{-1}$, while keeping the radial stress and pore pressure constant, i.e., drained conditions for both dry and water-saturated samples. In view of the estimated permeability of the Savonnières limestone (≈ 60 mD), the selected loading rate allows drainage of the pore fluid out of the water-saturated samples, which ensures the pore pressure of 0.5MPa is uniform during triaxial loading. The vertical stress is progressively increased up to and beyond the mechanical yield and failure of each rock sample. In addition, a dry and a water-saturated sample were tested under increasing confining pressure with no deviatoric stress until pore collapse and grain crushing take place.

For each rock sample, axial and radial strains, confining pressure, deviatoric stress, and pore pressure are monitored throughout the experiment. In addition, for the water-saturated samples, the evolution of water
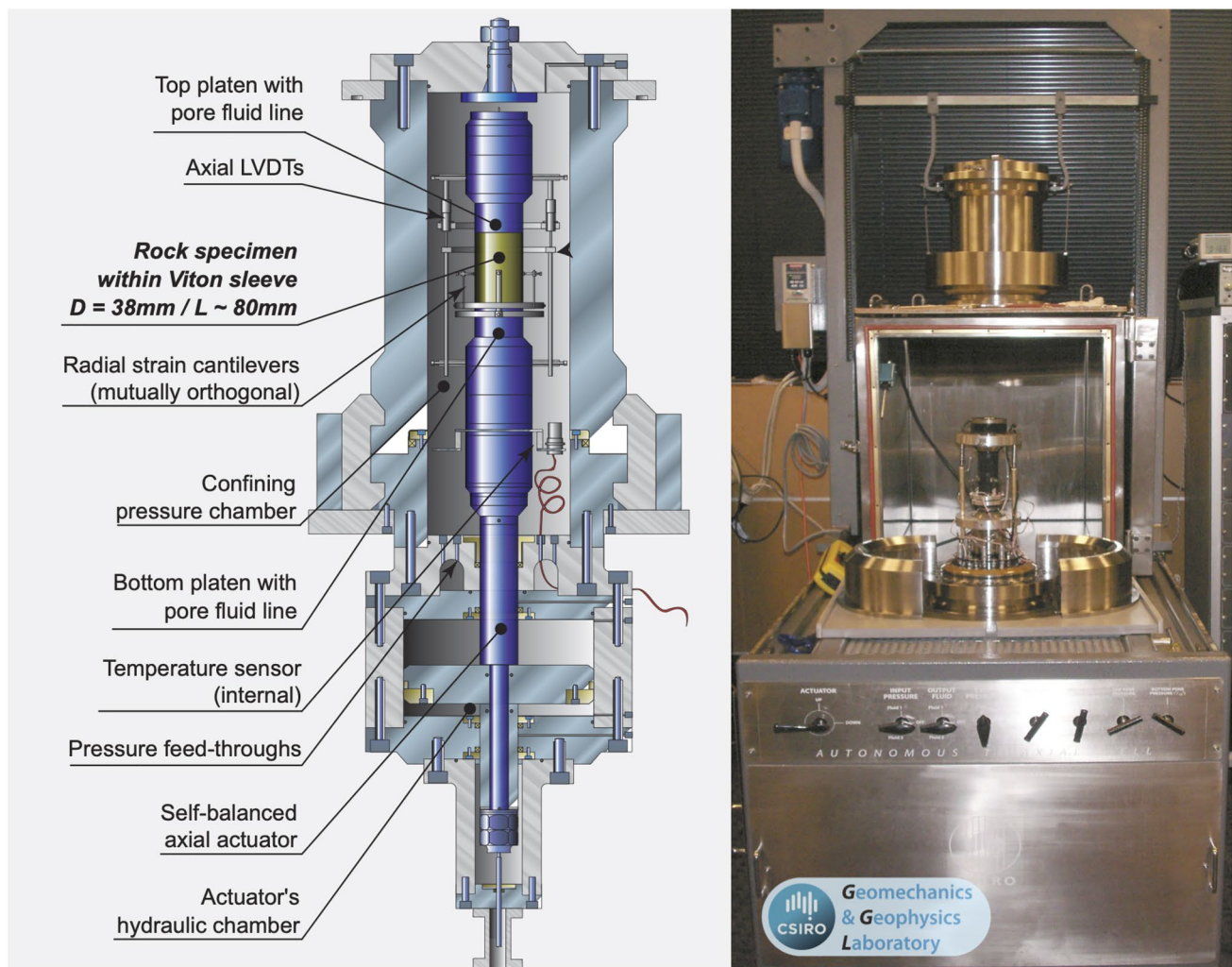
Fig. 2 Autonomous Triaxial Cell at CSIRO's Geomechanics and Geomechanics Laboratory. Figure reproduced from Sarout et al. (2014)
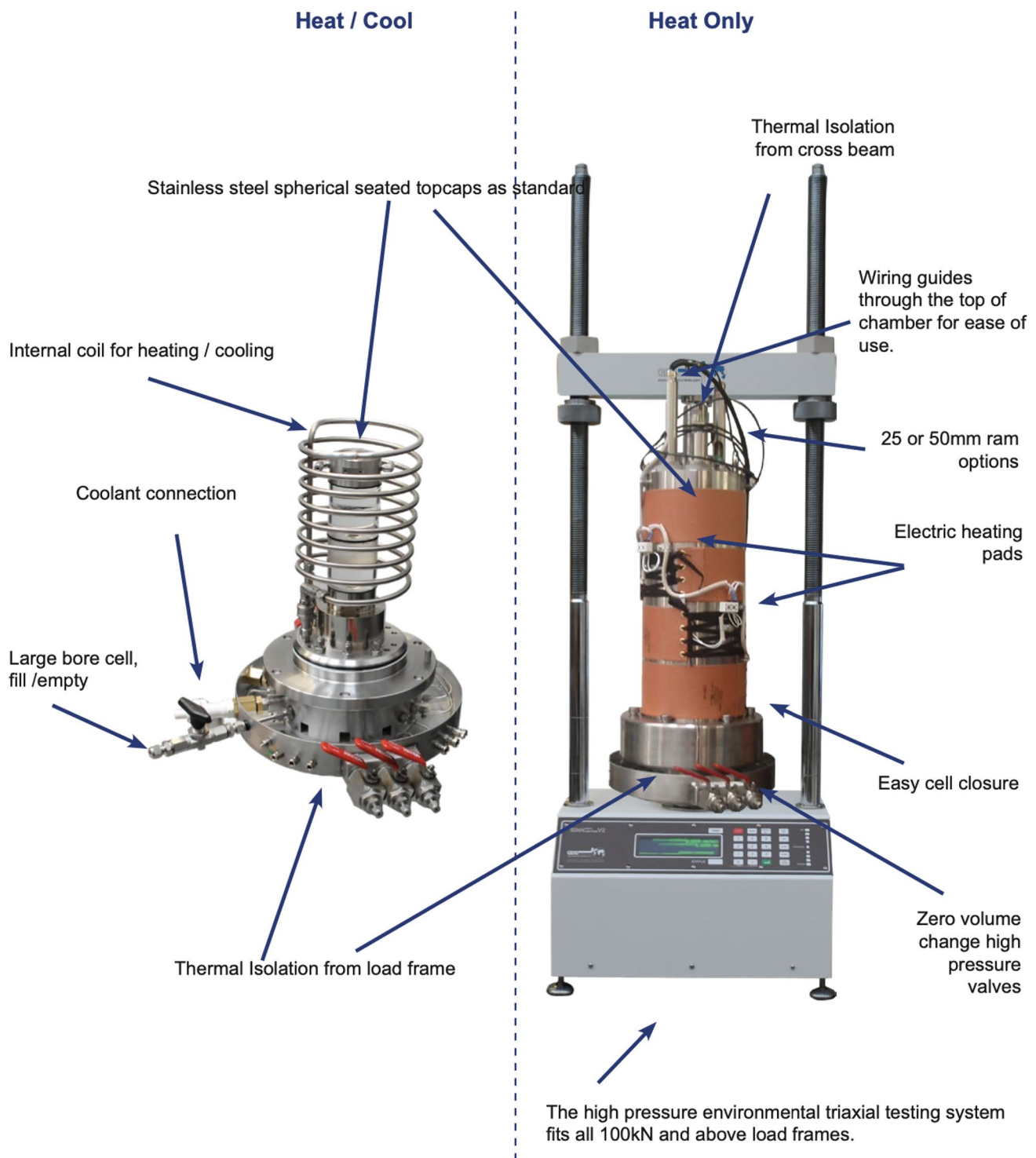
Fig. 3 Environmental Triaxial Automated System at Duke university. Figure modified from Ltd (2020)

permeability along the sample's axis under constant stress was measured. Finally, after triaxial testing, mechanical yield/failure, and subsequent stress release (unloading), the samples are imaged with a medical X-ray CT at room conditions in order to characterise the failure mode and associated strain localisation features (at the same resolution of 100 μm x 100 μm x 400 μm per voxel).

2.2.2 Triaxial Stress Vessels and Sample Instrumentation

In practice, two distinct triaxial vessels with similar capabilities were used: (i) the Autonomous Triaxial Cell (ATC) available in CSIRO's Geomechanics and Geophysics Laboratory: confining and pore pressure up to 70MPa, axial load up to 400kN, temperature up to 100°C (see Fig. 2); and (ii) the Environmental Triaxial Automated System (ETAS) available at Duke University: confining pressure and pore pressure up to 100MPa, axial load up to 100kN, temperature up to 100°C (see Fig. 3). Both vessels are designed to test cylindrical samples with a diameter D = 38mm, and a length L ≈ 76mm.

In the ATC, two vertical LVDTs are attached to the sides of the top and bottom platens (diametrically opposed locations) within the pressure chamber to monitor the sample's change in length. Two radial cantilevers are also attached to the sample's lateral surface at mid height, through the rubber sleeve, to monitor the radial deformation of the rock sample along mutually orthogonal directions within the horizontal plane. In the ETAS, LVDTs and radial gages are used to monitor the axial and the radial deformations, respectively. The recorded strain data represent the average deformation of the sample over its entire volume, and are used to calculate the volumetric strain, i.e., $\epsilon_{volumetric} = \epsilon_{axial} + 2 \cdot \epsilon_{radial}$

2.2.3 Permeability Estimation During Deformation

The constant-head permeability tests were performed in a triaxial cell under different conditions of confining pressure (5, 15 and 22 MPa) to measure the axial measurement of flows. Three advanced high pressure/volume controller (HPDPC) pumps have deployed for this experimental campaign, the first pump used to control the targeted confinement pressure. the other two pumps used to regulate the pore pressure (0.5 MPa) and to maintain a differential pressure for ($\Delta P = 0.25$ Mpa) for all tests and we measure the flow rate q.

Table 1 The table shows the stages where the permeability measurements were conducted for the three triaxial tests (5,15 and 22 MPa) effective confining pressure). Note that the pore pore and differential pressure were the same (0.5 0.25 MPa, respectively) for all measurements and we monitor the flow rate

Effective confining Pr. (MPa)	1st Measurement at % ϵ_{axial}	2nd Measurement at % ϵ_{axial}	3rd Measurement at % ϵ_{axial}	4th Measurement at % ϵ_{axial}
5	0	0.29	4.9	-
15	0	0.32	4.39	-
22	0	0.36	13.69	16.52

A distilled water was used in this study and the permeability measurements were conducted at different points of loading as shown in Table 1 and Fig. 8. For reference, a first water permeability measurement is conducted before starting the triaxial loading. After that, at specific values of axial strain, triaxial loading is momentarily halted to conduct additional permeability tests. Permeability is estimated using the steady-state method, i.e., a constant pressure gradient is imposed across the rock sample $\Delta P = 0.25$ Mpa), while the resulting flow rate is monitored until a steady regime is achieved. These permeability estimations are conducted during triaxial testing in the Environmental Triaxial Automated System (ETAS) with samples of Savonnières limestone 76 mm in length and 38 mm in diameter. The permeability k of the sample to water can be determined using Darcy's law as:

$$k = \frac{\mu L}{A} \frac{q}{\Delta P}, \tag{1}$$

where ΔP is the pressure difference across the sample (Pa), L is the length of the sample (m), μ is the viscosity of the fluid (Pa.s), q is the flow rate (m^3/s), and A is the cross sectional area of the sample.

2.2.4 X-Ray Computer Tomography (XRCT)

X-ray Computed Tomography is a technique used to image the internal volume of materials. The absorption of X-rays by materials is essentially related to their density, yielding 2D grey level/density maps that can be reconstructed into 3D density maps using existing algorithms and softwares (e.g., Osirix software by Pixmeo Ltd.). It is a valuable tool for evaluating the heterogeneities present in a rock sample (e.g., cracks, vuggs, fractures), and characterising its structure at the resolution allowed by the available XRCT scanner (typically sub-mm). All samples to be deformed in the triaxial stress vessel are imaged before (intact state) and after testing (post-mortem) using CSIRO's Siemens SOMATOM Definition AS scanner (see Figure 4), at an effective resolution of 100 μm x 100 μm x 400 μm.

3 Experimental Results

3.1 Stress–Strain Response

This section presents the results of the triaxial deformation experiments and the macroscopic mechanical behaviour of the Savonnières limestone, taking by convention compressive stress and compaction strain as positive. Figure 5 shows the resulting stress–strain curves of two representative triaxial testing scenarios (these experiments conducted at CSIRO laboratory), i.e., dry and water-saturated samples (drained)
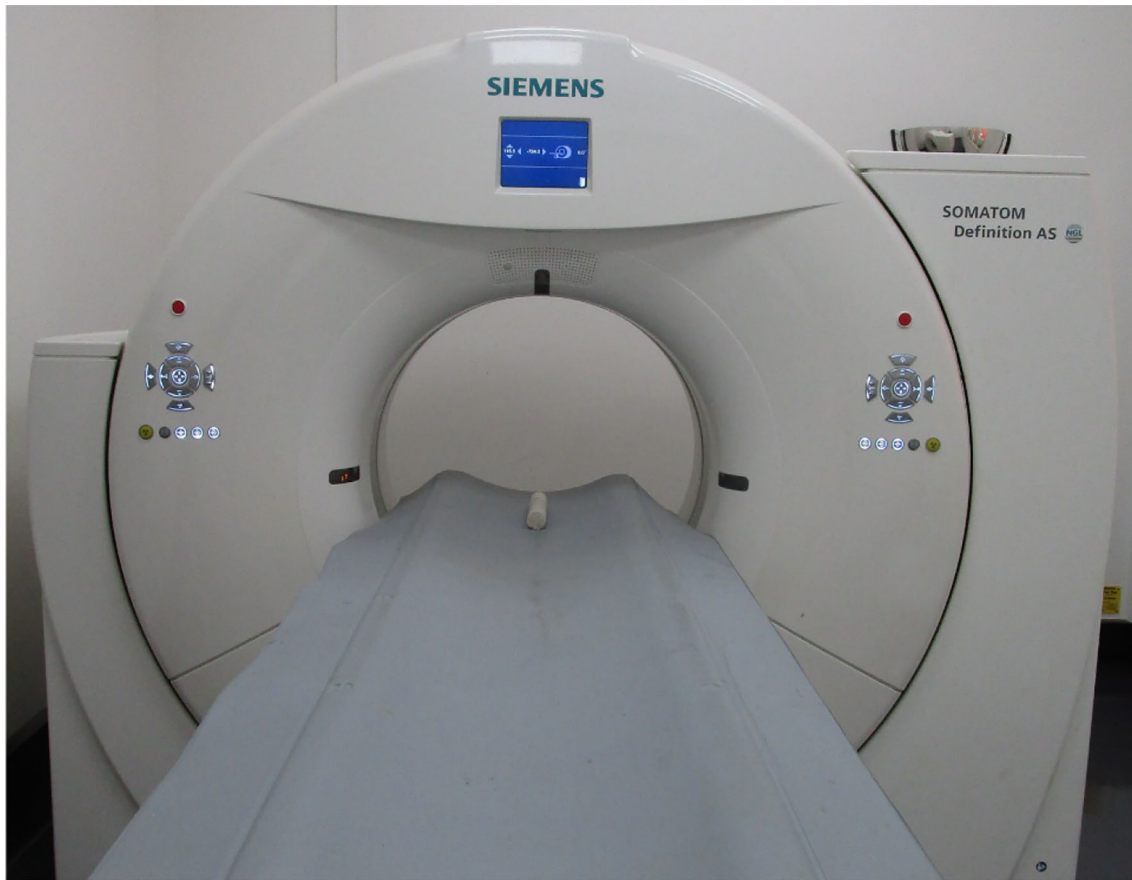
**Fig. 4** Siemens SOMATOM Definition AS medical X-ray CT scanner available at CSIRO

. Under increasing deviatoric stress, the Savonnières limestone deforms first in a quasi-linear and elastic manner. When the load is increased further, the rock progressively accumulates permanent inelastic strain (unrecoverable), and its stress–strain response deviates from linearity as mechanical yield/failure develops.

Figure 6 reports the stress–strain curves resulting from the effective confining pressure tests conducted on the dry and water-saturated (drained) samples with no applied deviatoric stress. The stress–strain response is quasi-linear and elastic until a threshold effective confining pressure is reached, i.e., $P_{eff} = 35$ and 46 MPa for the water-saturated and dry samples, respectively. In other words, a higher effective confining pressure is necessary to reach mechanical yield for the dry sample in comparison to the water-saturated (drained) one. In summary, it appears that the dry samples of Savonnières limestone are mechanically stronger than the water-saturated ones, whether they are subjected to a deviatoric stress loading, or to an isotropic stress loading.

### 3.2 Mechanical Yield/Failure Modes

Figure 7 shows the 3D density map of the rock samples obtained with a medical X-ray CT scanner after deformation under deviatoric loading. For both the dry and the water-saturated samples, the occurrence and geometrical attributes of strain localisation under deviatoric stress loading, and the associated yield/failure mode are strongly controlled by the effective confining pressure (depth) at which each triaxial test is conducted.

For the dry samples, shear bands with a high angle develop during the tests conducted at 1 and 5 MPa effective confining pressure, which is consistent with a brittle shear deformation regime. At 10 and 15 MPa effective confinement pressure we observe shear-enhanced compaction bands with a lower angle. In contrast, at 22 MPa the Savonnières limestone exhibits discrete compaction bands sub-orthogonal to the direction of maximum
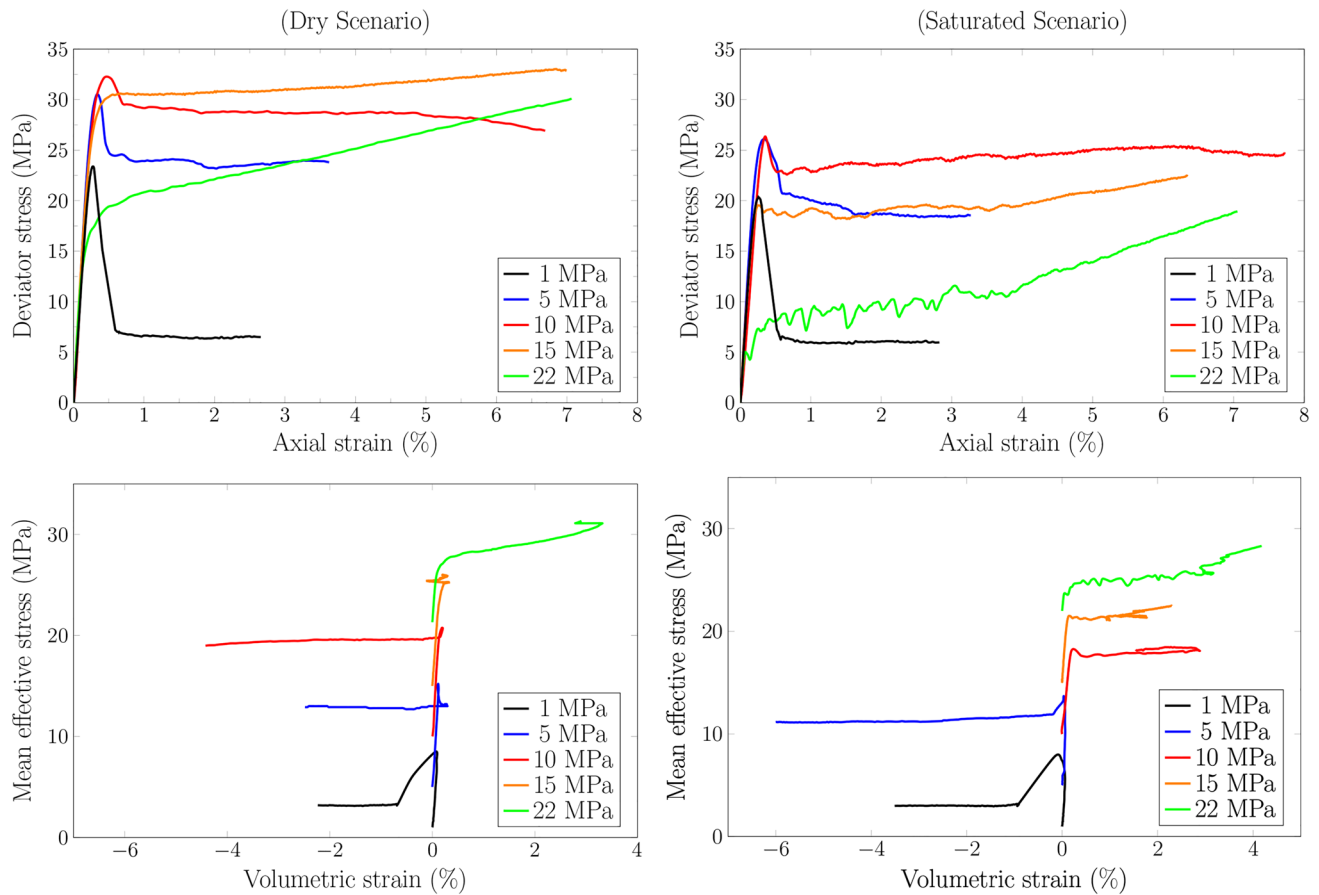
Fig. 5 Top: stress–strain data for multiple tests conducted at different effective confining pressures for both dry (left) and water-saturated (right) samples. Pore pressure is always constant and uniform at 0.5 MPa within each water-saturated sample). Bottom: Mean stress as a function of volumetric strain for a dry (left) and a water-saturated and drained sample of Savonnières (right), from experiments conducted at CSIRO Laboratory
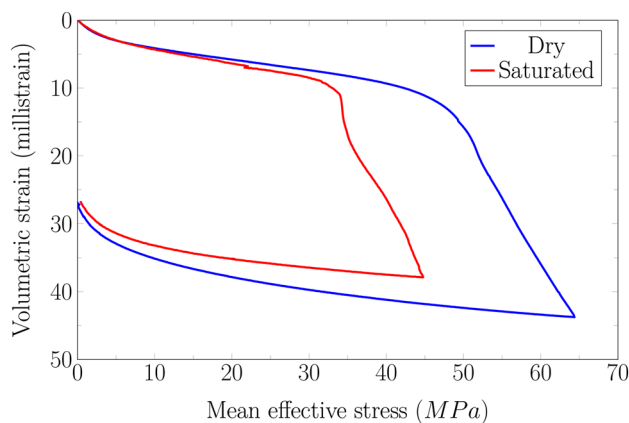

Fig. 6 Isotropic compression data for both dry and saturated condition

compressive stress. This suggests a progressive transition from a brittle shear to a more ductile deformation regime with increasing effective confining pressure.

A qualitatively similar brittle/ductile transition is observed for the water-saturated samples. However, the brittle/ductile transition seems to occur at a lower value of effective confining pressure compared to the dry samples. This observation is to be correlated with the fact that the presence of water in the pore space has been shown in the previous section to mechanically weaken the Savonnières limestone.

3.3 Permeability Evolution

Figure 8 shows the evolution of differential stress and permeability with axial strain for triaxial experiments conducted at Duke University at an effective confining pressure of 5,10 and 22 MPa. These data clearly show an overall reduction in water permeability with increasing axial strain during triaxial loading. Note that for the samples deformed at 5 or 10 MPa effective confining pressure, the brittle shear failure of the sample prevented any permeability measurement to be conducted beyond about
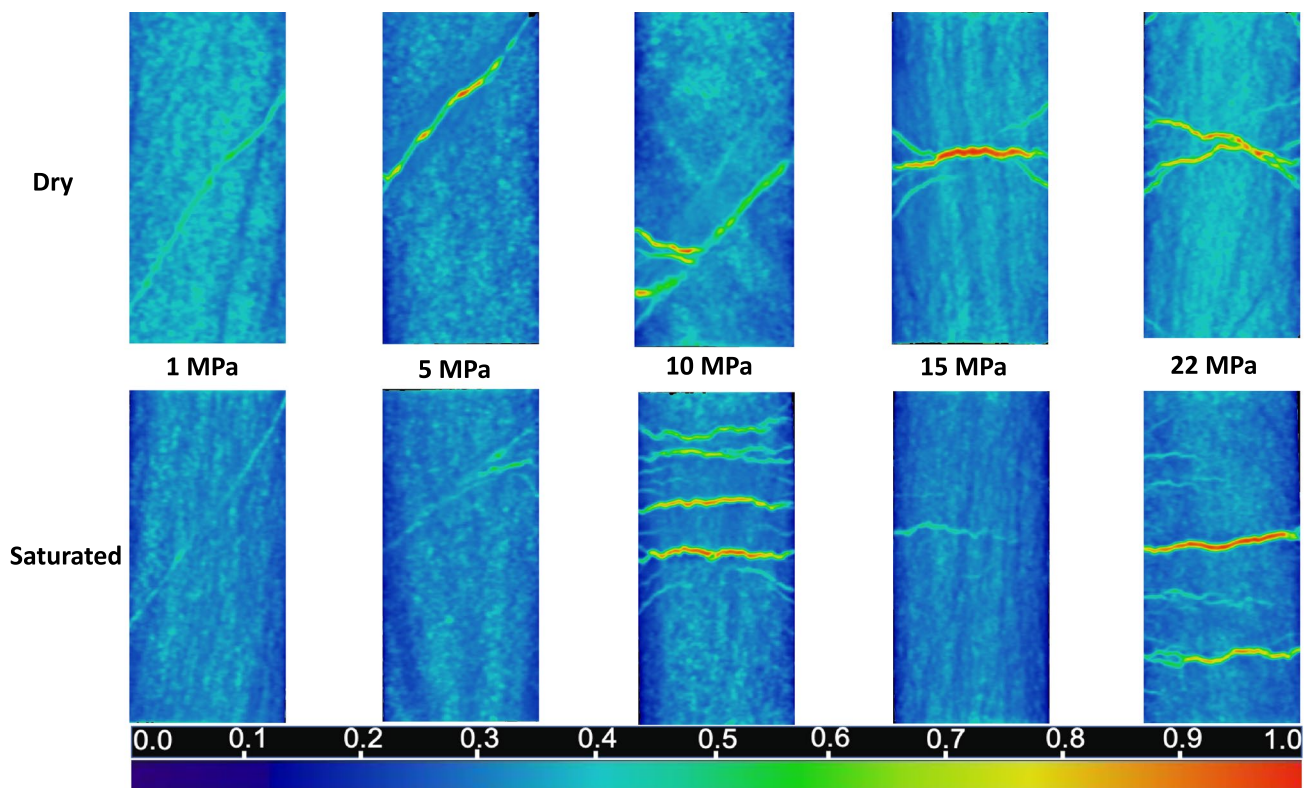
Fig. 7 3D porosity map of the rock samples obtained with a medical X-ray CT scanner after triaxial deformation at different effective confining pressures. Top row: dry samples. Bottom row: water-saturated drained samples. The dominant failure mode is changing with confinement from dilational (low angle to maximum compressive stress) to compactional (high angles to maximum compressive stress). Note that some of the samples detached at the localisation features due to the stress relaxation

5% axial strain (brittle failure by shear fracturing then slip along the shear fracture). For the sample deformed at 22 MPa effective confining pressure, a much larger axial strain value of nearly 18% could be reached in this semi-ductile deformation regime. At the highest axial strain values reached for this test, the compaction bands observed in the 3D X-ray CT images (see previous section) must have formed and can be confidently invoked as the cause of the observed permeability reduction from approximately 25 to 2 mD.

4 Discussion and Conclusion

4.1 Water Weakening

The stress at which the onset of inelastic strain occurs is called the yield point and can be identified as the deviation from the linear-elastic response (Jaeger et al. 2007; Parker 2003; Bedford et al. 2018). Deforming rocks, both in the compaction and dilation regimes, are pressure sensitive, that means the stress at which yield occurs varies with pressure. The yield curve can, therefore, be defined in the so-called P-Q stress space as the locus of the yield point obtained for each triaxial test conducted at a different effective confining pressure. P is the mean effective stress: P $= (\sigma_1 + \sigma_2 + \sigma_3)/3 - p_f$, where p_f is the pore fluid pressure, and σ_i are the principal stresses. Q is the differential stress: Q $= \sigma_1 - \sigma_3$.

Figure 9 compares the yield envelopes obtained for the dry and water-saturated (drained) tests reported in Figs. 5 (triaxial loading) and 6 (isotropic loading). We observe that the presence of water instead of air in the pore space of the Savonnières limestone reduces the mechanical strength of the rock for both triaxial and isotropic loading modes, and for all effective confining pressures tested. This results in a significant shrinkage of the yield envelope associated with exposure to the saturating water, and this strength reduction is more pronounced in the transition toward the ductile regime at higher effective confining pressures. In general, the role of the saturating fluid has a significant affect on the mechanical properties (yield stress, creep, etc.) as shown by Gennaro and Pereira (2013), the key example of the water weakening is what had occurred at the Ekofisk Field in the Norwegian sector of the North Sea Teufel et al. (1991); Sylte et al. (1999).
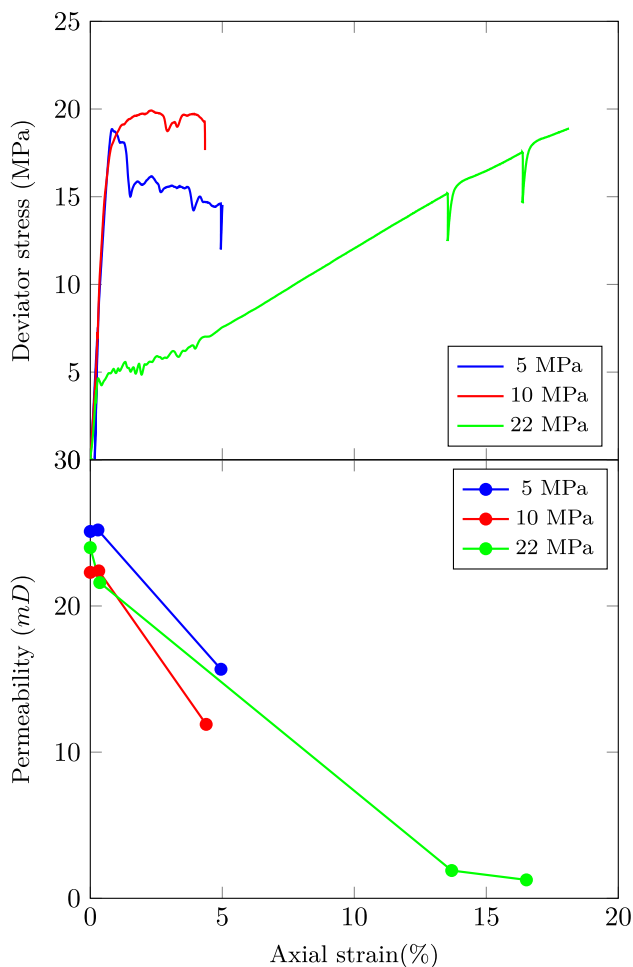
Fig. 8 Experimental data for Savonnières samples where the differential stress and permeability are plotted against axial strain for multiple effective confining pressures. Experiments conducted at Duke University

4.2 Failure Mode and Compaction Bands

The post-mortem XRCT images of the samples subjected to triaxial loading illustrate the transition of the strain localisation structure within the samples from shear fracturing at low angle to the maximum (vertical) compressive stress, to sub-orthogonal shear-enhanced compaction with increasing effective confining pressure. This transition from brittle faulting to cataclastic flow can be correlated with the stress–strain data reported in Fig. 5, i.e., transition from strain softening at low confinement pressure to strain hardening at high confinement pressure. The onset of shear-enhanced compaction and development of cataclastic flow also correlates well with the considerable permeability reduction observed (one order of magnitude) as shown in Fig. 8. These correlated observations strongly suggest the formation of sub-horizontal compaction bands, effectively reducing the vertical permeability of the rock.

Figure 10 shows the comparison between the permeability data obtained on intact samples of Savonnières limestone under hydrostatic loading using nitrogen and the permeability data that obtained using a triaxial apparatus using water as pore fluid for three confinements (5, 10, 22 MPa). Those results show a difference of a factor 3 between the two measurement techniques (about 25 mD at 5,10,22 MPa with water, about 60mD using nitrogen).

This could be due to the difference in the effective pressure state the samples were subjected to during each permeability measurement (2 MPa with nitrogen, and 5 MPa or more with water), or could be due to the change in microstructure associated with the water weakening that takes place when we saturate the rock's pore space with water. We further speculate that the observed weakening and possible micro-structural changes are due to chemical or capillary/ surface energy forces as often discussed in the literature,

Fig. 9 Yield envelope for both scenarios (dry, saturated) showing the values of the triaxial tests as well as the isotropic compression tests. The seemingly distorted shapes at the cap are due to the fact that values of the isotropics tests, which are stress controlled, are larger than the values obtained from the triaxial tests, which are displacement controlled. All yield points are visually identified where the corresponding stress–strain curves deviate from their initial linear elastic response (Jaeger et al. 2007; Parker 2003; Bedford et al. 2018)
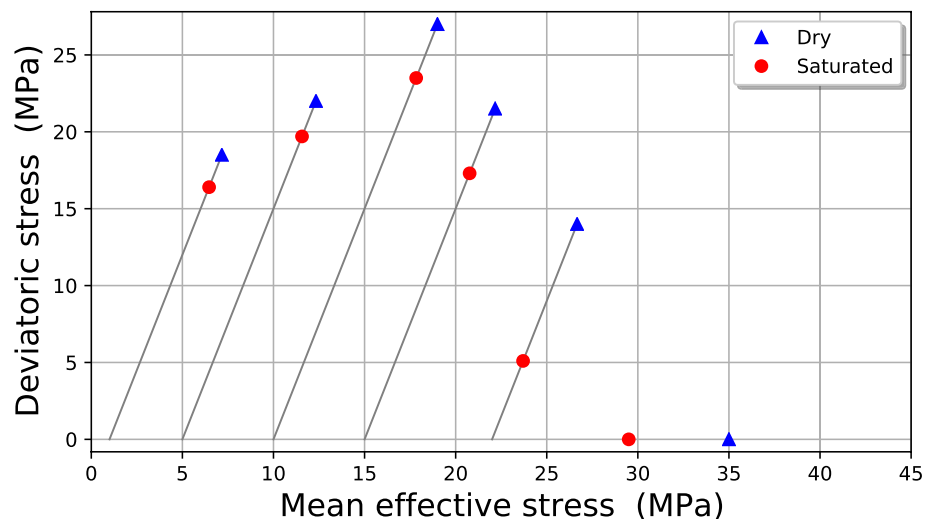
Fig. 10 Permeability as function of mean effective stress measured by a) automatic porosity permeability apparatus by nitrogen on intact Savonnières at hydrostatic condition for multiple effective pressures, b) triaxial apparatus for three confinements pressure (5, 10,22 MPa) using water as pore fluid
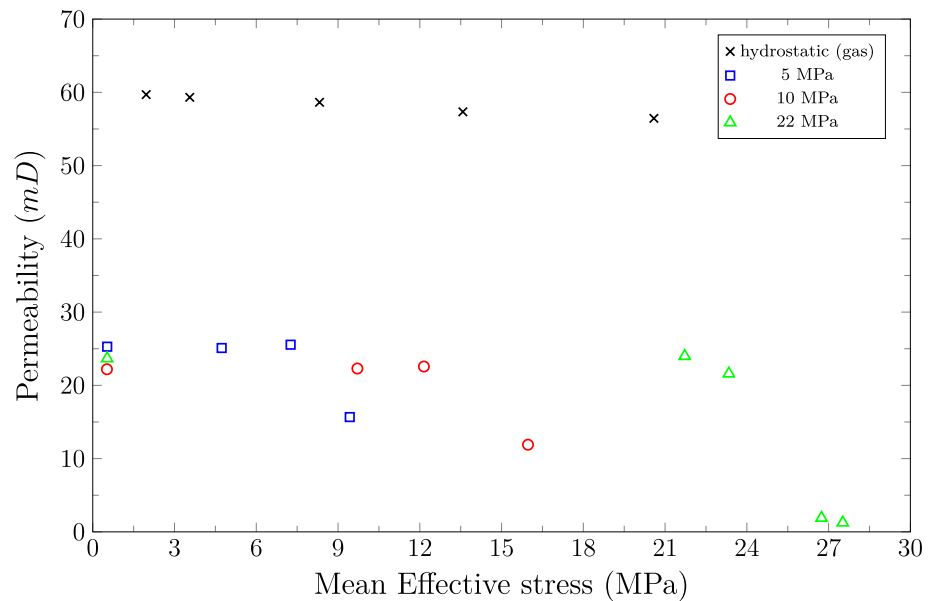
even though unfortunately, the data available so far are insufficient to discriminate conclusively between these possible mechanisms.

References

Abdallah Y, Sulem J, Bornert M, Ghabezloo S, Stefanou I (2021) Compaction banding in high-porosity carbonate rocks: 1 experimental observations. J Geophys Res Solid Earth. https://doi.org/10.1029/2020JB020538

Atkinson BK, Meredith PG (1987) 11 - experimental fracture mechanics data for rocks and minerals. In: ATKINSON BK. (ed.) Fracture Mechanics of Rock, pp. 477–525. Academic Press, London. https://doi.org/10.1016/B978-0-12-066266-1.50016-8

Baud P, Schubnel A, Wong T-f (2000) Dilatancy, compaction, and failure mode in solnhofen limestone. J Geophys Res 105:19289–19304. https://doi.org/10.1029/2000JB900133

Baud P, Zhu W, Wong T-F (2000) Failure mode and weakening effect of water on sandstone. J Geophys Res 105:16371–16390. https://doi.org/10.1029/2000JB900087

Bedford J, Faulkner D, Leclére H, Wheeler J (2018) High-resolution mapping of yield curve shape and evolution for porous rock: The effect of inelastic compaction on porous bassanite. J Geophys Res Solid Earth. https://doi.org/10.1002/2017JB015250

Cadoret T, Marion D, Zinszner B (1995) Influence of frequency and fluid distribution on elastic wave velocities in partially saturated limestones. J Geophys Res Solid Earth 100(B6):9789–9803

Colback P, Wiid B (1965) The influence of moisture content on the compressive strength of rocks. Geophysics

Croize D, Renard F, Gratier J-P (2013) Compaction and porosity reduction in carbonates: A review of observations, theory, and experiments. Adv Geophys 54:181–238. https://doi.org/10.1016/B978-0-12-380940-7.00003-2

Dautriat J, Gland N, Guelard J, Dimanov A, Raphanel J (2009) Axial and Radial Permeability Evolutions of Compressed Sandstones: End Effects and Shear-band Induced Permeability Anisotropy. Pure Appl Geophys 166:1037–1061. https://doi.org/10.1007/s00024-009-0495-0

David C, Dautriat J, Sarout J, Delle Piane C, Menéndez B, Macault R, Bertauld D (2015) Mechanical instability induced by water weakening in laboratory fluid injection tests. J Geophys Res Solid Earth 120(6):4171–4188. https://doi.org/10.1002/2015JB011894

Dimanov A, Dautriat J, Gland N, Raphanel J (2011) Hydromechanical behavior of heterogeneous carbonate rock under proportional triaxial loadings. J Geophys Res 116(B01205):10–10292009000830. https://doi.org/10.1029/2009JB000830

Erguler ZA, Ulusay R (2009) Water-induced variations in mechanical properties of clay-bearing rocks. Int J Rock Mechan Mining Sci 46(2):355–370. https://doi.org/10.1016/j.ijrmms.2008.07.002

Fortin J, Guéguen Y, Schubnel A (2007) Effects of pore collapse and grain crushing on ultrasonic velocities and vp/vs. J Geophys Res Solid Earth. https://doi.org/10.1029/2005JB004005

Fortin J, Schubnel A, Gueguen Y (2005) Elastic wave velocities and permeability evolution during compaction of bleuswiller sandstone. Int J Rock Mechan Mining Sci 42:873–889. https://doi.org/10.1016/j.ijrmms.2005.05.002

Fronteau G, Moreau C, Thomachot-Schneider C, Barbin V (2010) Variability of some lutetian building stones from the paris basin, from characterisation to conservation. Eng Geol 115(3):158–166. https://doi.org/10.1016/j.enggeo.2009.08.001

De Gennaro V, Pereira JM (2013) A viscoplastic constitutive model for unsaturated geomaterials. Comput Geotech 54:143–151. https://doi.org/10.1016/j.compgeo.2013.06.005

Ghabezloo S, Sulem J, Guédon S, Martineau F (2009) Effective stress law for the permeability of a limestone. Int J Rock Mechan Mining Sci 46(2):297–306. https://doi.org/10.1016/j.ijrmms.2008.05.006

Gouze P, Luquot L (2011) X-ray microtomography characterization of porosity, permeability and reactive surface changes during dissolution. J Contamin Hydrol 120–121:45–55. https://doi.org/10.1016/j.jconhyd.2010.07.004

Gratier J-P, Renard F, Labaume P (1999) How pressure solution creep and fracturing processes interact in the upper crust to make it behave in both a brittle and viscous manner. J Stru Geol 21(8):1189–1197. https://doi.org/10.1016/S0191-8141(99)00035-8

Grgić D (2011) Influence of co_2 on the longterm chemomechanical behavior of an oolitic limestone. J Geophys Res. https://doi.org/10.1029/2010JB008176

Halbouty MT (2003) Giant oil and gas fields of the decade 1990-1999. Am Assoc Petrol Geol

Hawkins AB, McConnell BJ (1992) Sensitivity of sandstone strength and deformability to changes in moisture content. Quarterly J Eng Geol Hydrogeol 25(2):115–130. https://doi.org/10.1144/GSL.QJEG.1992.025.02.05

Issen KA (2002) The influence of constitutive models on localization conditions for porous rock. Eng Fract Mechan 69(17):1891–1906. https://doi.org/10.1016/S0013-7944(02)00067-X

Jaeger JC, Cook NGW, Zimmerman R (2007) Fundamentals of rock mechanics. Wiley

Kodaka T, Oka F, Kitahara H, Ohta H, Otani J (2017) Observation of compaction bands under triaxial conditions for diatomaceous mudstone, pp. 69–75. https://doi.org/10.1201/9781315106656-12

Leuthold J, Gerolymatou E, Vergara MR, Triantafyllidis T (2021) Effect of compaction banding on the hydraulic properties of porous rock: part i - experimental investigation. Rock Mechan Rock Eng 54(6):2671–2683. https://doi.org/10.1007/s00603-021-02427-w

Ltd GDS (2020) Environmental Triaxial Automated System. GDS Instruments, Unit 32 Murrell Green Business Park London Road. GDS Instruments

Moh BK (2008) Determination of the vuggy porosity of some oolitic building limestones and the practical implications

Orowan E (1944) The fatigue of glass under stress. Nature 154:341–343

Papamichos E, Vardoulakis I, Ouadfel H (1993) Permeability reduction due to grain crushing around a perforation. Int J Rock Mechan Mining Sci Geomechan Abstracts 30(7):1223–1229. https://doi.org/10.1016/0148-9062(93)90099-Y

Parker SP (2003) Mcgraw-hill dictionary of scientific and technical terms. McGraw-Hill New York, 2380

Paterson M, Wong T-f (2005) Experimental rock deformation - the brittle field. Experim Rock Deform Brittle Field. https://doi.org/10.1007/b137431

Pimienta L, Sarout J, Esteban L, David C, Clennell MB (2017) Pressure-dependent elastic and transport properties of porous and permeable rocks: Microstructural control. J Geophys Res Solid Earth 122(11):8952–8968. https://doi.org/10.1002/2017JB014464

Qajar J, Francois N, Arns CH (2013) Microtomographic Characterization of Dissolution-Induced Local Porosity Changes Including Fines Migration in Carbonate Rock. SPE J 18(03):545–562. https://doi.org/10.2118/153216-PA

Rebinder PA, Schreiner LA, Zhigach KF (1948) Hardness Reducers in Drilling : a Physico-chemical Method of Facilitating the Mechanical Destruction of Rocks During Drilling. Council for Scientific and Industrial Research, Melbourne

Risnes R, Madland MV, Hole M, Kwabiah NK (2005) Water weakening of chalk-mechanical effects of water-glycol mixtures. J Petrol Sci Eng 48(1):21–36. https://doi.org/10.1016/j.petrol.2005.04.004

Roehl P, Choquette P (1986) Carbonate petroleum reservoirs. Geolog Magaz 123(6):712–713. https://doi.org/10.1017/S0016756800024365

Sari M, Alevizos S, Poulet T, Lin J, Veveakis M (2020) A visco-plastic framework for interface processes in sedimentary reservoir rocks at hpht conditions. Geomechan Energy Environm. https://doi.org/10.1016/j.gete.2019.100165

Sarout J, Esteban L, Delle Piane C, Maney B, Dewhurst DN (2014) Elastic anisotropy of Opalinus Clay under variable saturation and triaxial stress. Geophys J Int 198(3):1662–1682. https://doi.org/10.1093/gji/ggu231

Schlumberger (2007) Carbonate reservoirs: meeting unique challenges to maximize recovery. Technical report, Schlumberger, Houston

Schmitt L, Forsans T, Santarelli FJ (1994) Shale testing and capillary phenomena. Int J Rock Mechan Mining Sci Geomechan Abstracts 31(5):411–427. https://doi.org/10.1016/0148-9062(94)90145-7

Shulakova V, Sarout J, Pimienta L, Lebedev M, Mayo S, Clennell MB, Pervukhina M (2017) Effect of supercritical $co2$ on carbonates: Savonniéres sample case study. Geophys Prospect 65(1):251–265. https://doi.org/10.1111/1365-2478.12369

Stefanou I, Sulem J (2014) Chemically induced compaction bands: Triggering conditions and band thickness. J Geophys Res Solid Earth 119(2):880–899. https://doi.org/10.1002/2013JB010342

Sulem J, Vardoulakis I (1995) Bifurcation analysis in geomechanics. CRC Press

Sylte J, Thomas L, Rhett D, Bruning D, Nagel N (1999) Water induced compaction in the ekofisk field. In: SPE Annual Technical Conference and Exhibition. https://doi.org/10.2118/56426-MS

Teufel LW, Rhett DW, Farrell HE (1991) Effect of reservoir depletion and pore pressure drawdown on in situ stress and deformation in the ekofisk field, north sea. In: The 32nd US Symposium on Rock Mechanics (USRMS)

Tserkovnyak Y, Johnson DL (2002) Can one hear the shape of a saturation patch. Geophys Res Lett 29:12–1124. https://doi.org/10.1029/2001gl014709

Vajdova V, Baud P, Wong T-f (2004) Compaction, dilatancy, and failure in porous carbonate rocks. J Geophys Res Solid Earth. https://doi.org/10.1029/2003JB002508

Vik B, Bastesen E, Skauge A (2013) Evaluation of representative elementary volume for a vuggy carbonate rock-part: Porosity, permeability, and dispersivity. J Petrol Sci Eng 112:36–47. https://doi.org/10.1016/j.petrol.2013.03.029

Vo-Thanh D (1995) Influence of fluid chemistry on shear-wave attenuation and velocity in sedimentary rocks. Geophys J Int 121(3):737–749. https://doi.org/10.1111/j.1365-246X.1995.tb06435.x

Vàsàrhelyi B (2005) Statistical analysis of the influence of water content on the strength of the miocene limestone. Rock Mechan Rock Eng 38(1):69–76. https://doi.org/10.1007/s00603-004-0034-3

Wong T-f, Baud P (2012) The brittle-ductile transition in porous rock: A review. J Struc Geol 44:25–53. https://doi.org/10.1016/j.jsg.2012.07.010

Wong T-f, David C, Zhu W (1997) The transition from brittle faulting to cataclastic flow in porous sandstones: Mechanical deformation. J Geophys Res Solid Earth 102(B2):3009–3025. https://doi.org/10.1029/96JB03281

Zhang X, Spiers CJ (2005) Compaction of granular calcite by pressure solution at room temperature and effects of pore fluid chemistry. Int J Rock Mechan Mining Sci 42(7):950–960. https://doi.org/10.1016/j.ijrmms.2005.05.017

Zhang X, Spiers CJ, Peach CJ (2010) Compaction creep of wet granular calcite by pressure solution at 28°c to 150°c. J Geophys Res Solid Earth. https://doi.org/10.1029/2008JB005853

Zhu W, Baud P, Wong T-f (2010) Micromechanics of cataclastic pore collapse in limestone. J Geophys Res. https://doi.org/10.1029/2009JB006610

Zhu W, Wong T-f (1997) Shear-enhanced compaction in sandstone under nominally dry and water-saturated conditions. Int J Rock Mechan Mining Sci 34(3):364–136412. https://doi.org/10.1016/S1365-1609(97)00030-0

Zhu W, Montési LGJ, Wong T-F (2002) Effects of stress on the aniso-tropic development of permeability during mechanical compaction of porous sandstones. Geological Society, London, Special Publications 200(1):119–136. https://doi.org/10.1144/GSL.SP.2001.200.01.08